

SUPPLEMENTARY MATERIAL FOR:

# **Recognition between a short unstructured peptide and a partially folded fragment leads to the thioredoxin fold sharing native-like dynamics**

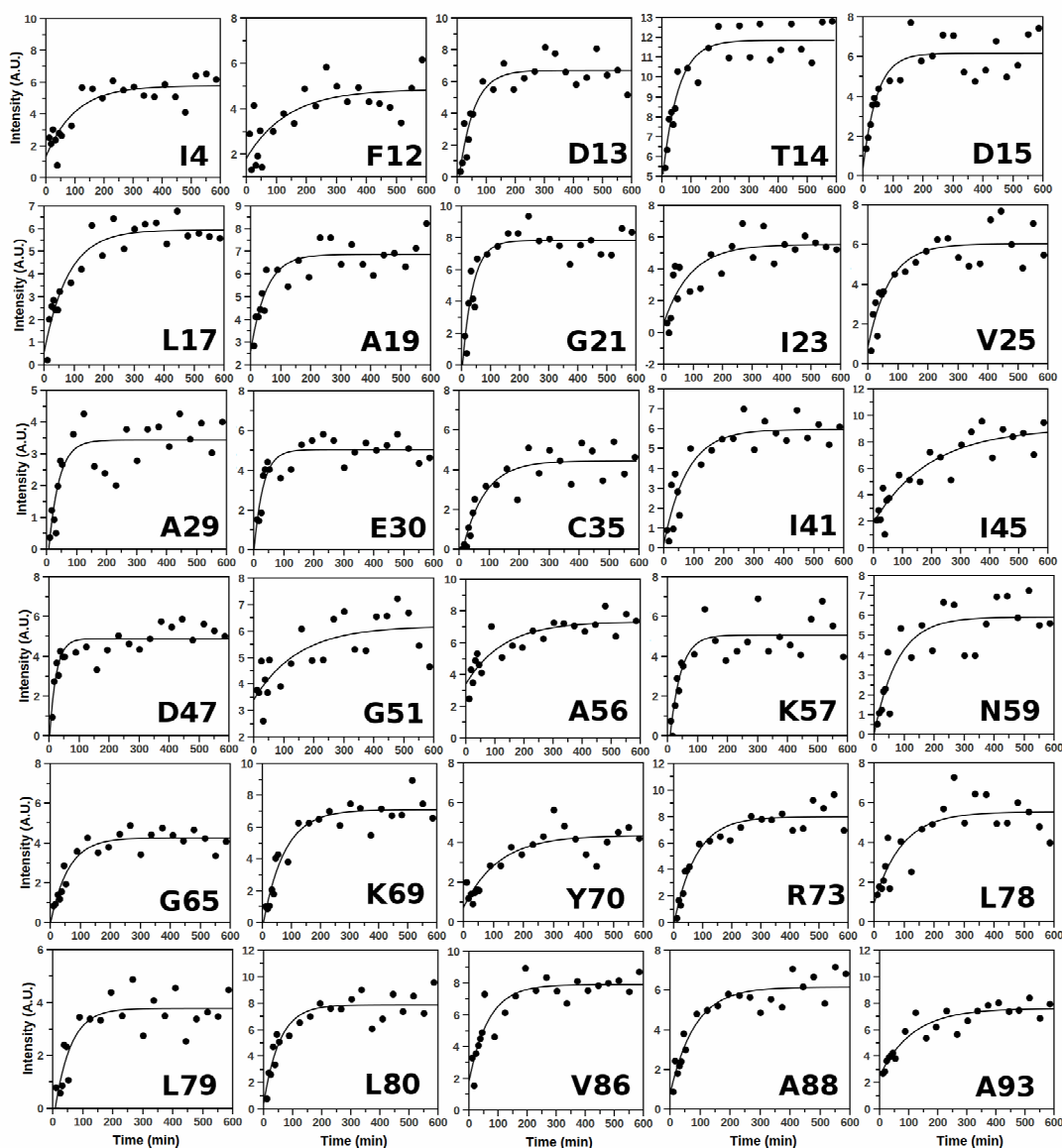
**Andrés Binolfi,<sup>2</sup> Claudio O. Fernández,<sup>2,4</sup> Mauricio P. Sica,<sup>3</sup> José M. Delfino,<sup>1\*</sup> and Javier Santos<sup>1,3\*</sup>**

<sup>1</sup>Departamento de Química Biológica e Instituto de Química y Fisicoquímica Biológicas (IQUIFIB), Facultad de Farmacia y Bioquímica, Universidad de Buenos Aires, Junín 956, C1113AAD Buenos Aires, Argentina

<sup>2</sup>Instituto de Biología Molecular y Celular de Rosario, Consejo Nacional de Investigaciones Científicas y Técnicas, Universidad Nacional de Rosario, Suipacha 531, S2002LRK Rosario, Argentina

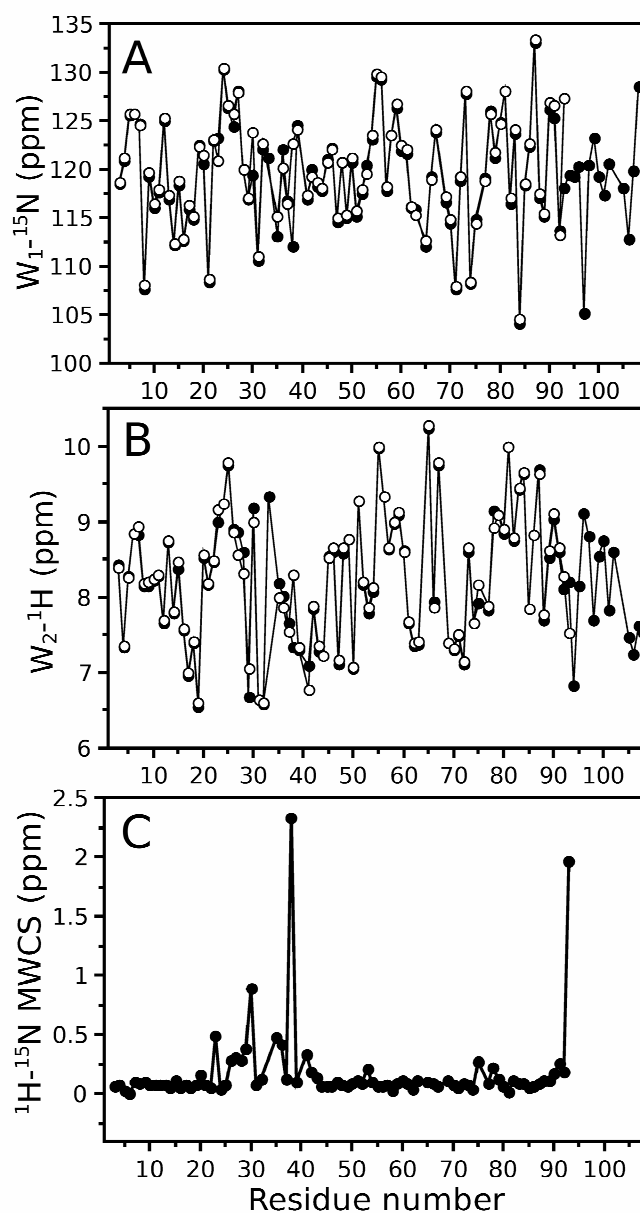
<sup>3</sup>Department of Science and Technology, University of Quilmes, Roque Sáenz Peña 352, B1876XD Bernal, Buenos Aires, Argentina

<sup>4</sup>Department of NMR-based Structural Biology, Max Planck Institute for Biophysical Chemistry, Am Fassberg 11, D-37077 Göttingen, Germany and DFG Research Center for the Molecular Physiology of the Brain (CMPB), Göttingen, Germany



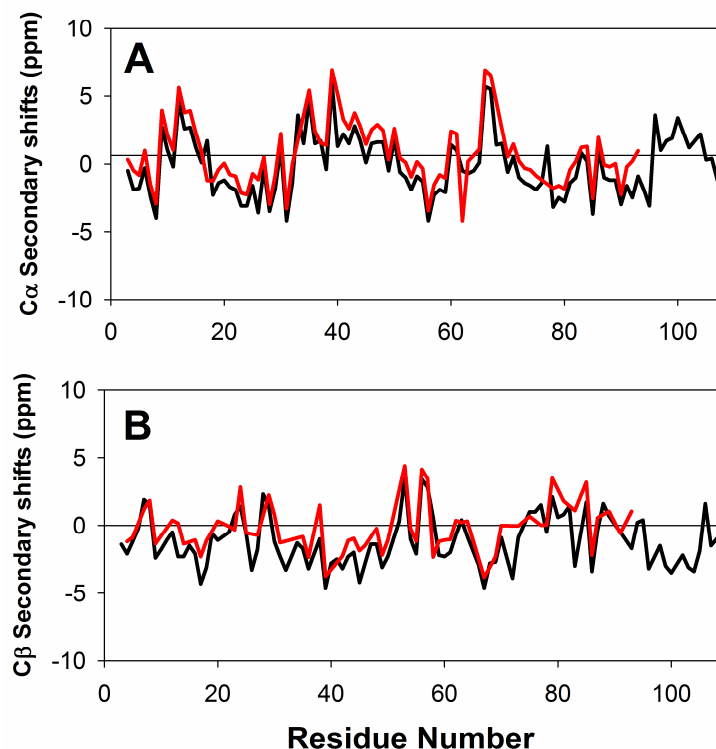
**Figure S1.** Reaction of complex TRX1-93/TRX94108 formation followed by real-time NMR. Intensities of  $^1\text{H}$ - $^{15}\text{N}$  cross-peaks for residues, measured from  $^1\text{H}$ - $^{15}\text{N}$  HET-SOFAST experiments run under the experimental conditions indicated in Figure 1 were plotted as a function of reaction time ( $t = 0$  being the time when mixing of peptide and fragment occurs). After global regression analysis by fitting one exponential component to each kinetics, the curves were plotted corresponding to residues: 4, 12, 13, 14, 15, 17, 19, 21, 23, 25, 29, 30, 35, 41, 45, 47, 51, 56, 57, 59, 65, 69, 70, 73, 78, 79, 80, 86, 88,

and 93. These residues were selected to follow the progress of their cross-peak intensities along the reaction time, because they are well resolved in the final spectrum.

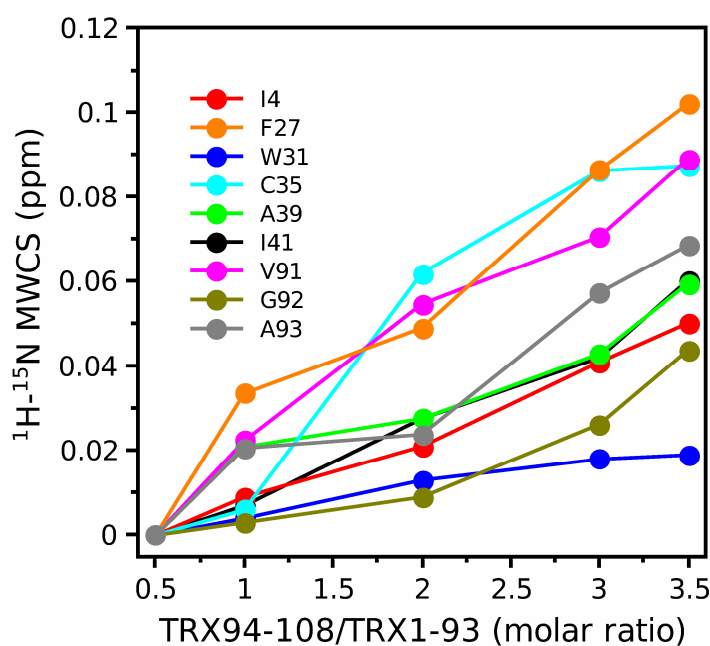


**Figure S2.** Comparison of chemical shifts for the reduced form of fragment  $^{13}\text{C}/^{15}\text{N}$  TRX1-93 (500  $\mu\text{M}$ ) in complex with peptide  $^{12}\text{C}/^{14}\text{N}$  TRX94-108 (1.5 mM) (○), and wild-type TRX (●).  $^{15}\text{N}$  (A),  $^1\text{H}$  amide (B). The mean-weighted  $^1\text{H}\text{-}^{15}\text{N}$  chemical shifts difference (MWCS in ppm) as a function of residue number is plotted in (C). Normalized MWCS was calculated as follows:  $MWCS = [\Delta H^2 + (\Delta N/5)^2]^{1/2}$ ,

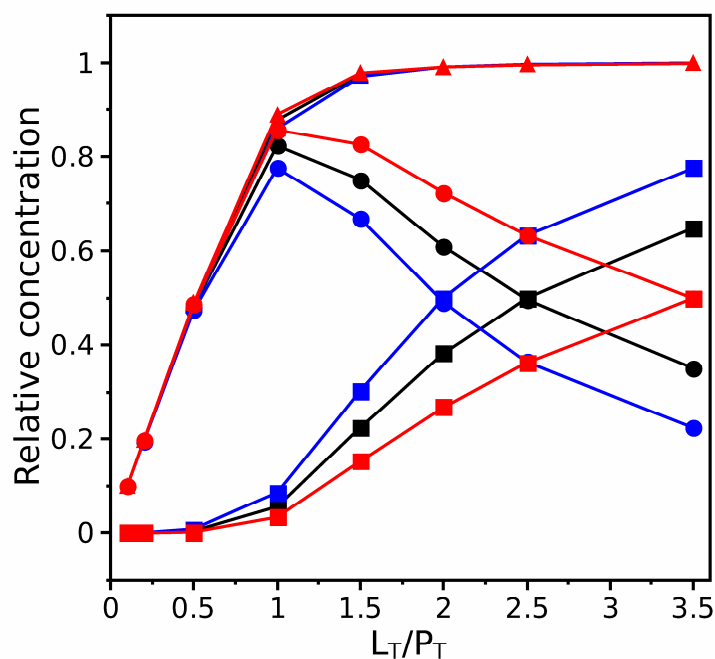
where  $\Delta H$  and  $\Delta N$  are the chemical shifts differences between the complex and wild-type TRX. The buffer was 20 mM Tris-HCl, 100 mM NaCl, 1 mM DTT, pH 7.3 at 20 °C.



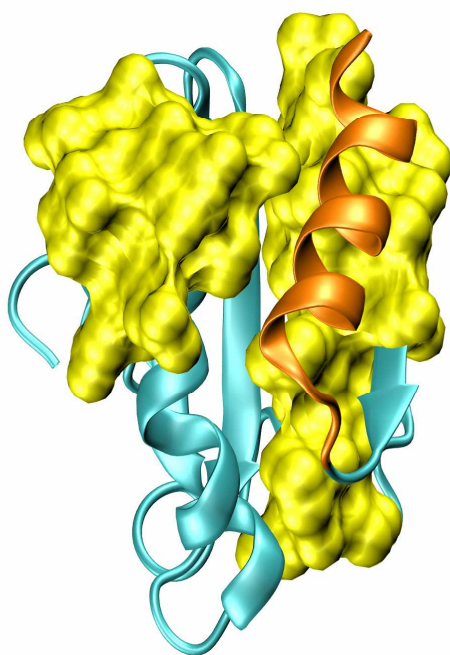
**Figure S3.** C $\alpha$  (A) and C $\beta$  (B) secondary shifts for full-length TRX (black) and the complex TRX1-93/94-108 (red). Chemical shifts values for full-length TRX were those reported by Chandrasekhar et al.<sup>1</sup>. The plots show that the secondary shifts of both protein species (up to residue 93) are very similar, indicating that the structural features of the complex strongly resemble those of the full-length protein. The slightly different offset between both datasets ( $\sim 0.5$  ppm) likely arises from the different solution conditions in both studies and/or the reference compounds used: DSS in this work and tetra methyl silane (TMS) and NH<sub>3</sub> in Chandrasekhar et al.<sup>1</sup>.



**Figure S4.** Amino acid residues that change their chemical shifts upon titration of  $^{15}\text{N}$  uniformly labeled fragment TRX1-93 with unlabeled peptide TRX94-108. For cross-peaks corresponding to residues I4, F27, W31, C35, A39, I41, V91, G92 and A93, the mean-weighted  $^1\text{H}$ - $^{15}\text{N}$  chemical shifts (in ppm) were calculated as  $^1\text{H}$ - $^{15}\text{N}$  MWCS =  $[\Delta\text{H}^2 + (\Delta\text{N}/5)^2]^{1/2}$ , where  $\Delta\text{H}$  and  $\Delta\text{N}$  are the differences in chemical shift observed for  $^1\text{H}$  and  $^{15}\text{N}$  relative to the minimal peptide/fragment assayed (0.5:1). Dialyzed fragment  $^{15}\text{N}$ -TRX1-93 (100  $\mu\text{M}$ , final concentration) was mixed with peptide TRX94-108 (at peptide/fragment molar ratios of 0.5:1, 1:1, 2:1, 3:1, 3.5:1).  $^1\text{H}$ - $^{15}\text{N}$ - HSQC spectra were acquired after at least 16 h of incubation at room temperature.

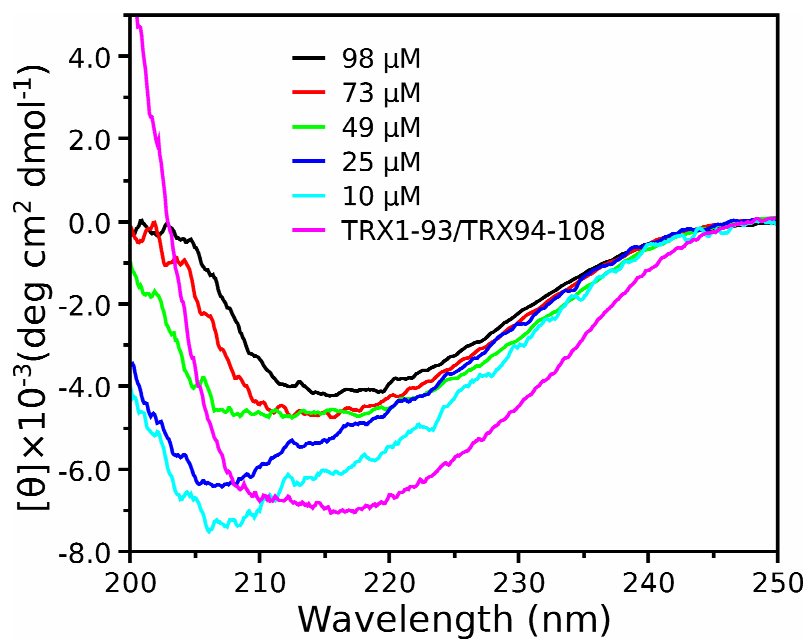


**Figure S5.** Simulation of two coupled binding equilibria between fragment TRX1-93 (P) and peptide TRX94-108 (L). The systems  $P + L \leftrightarrow PL$  and  $PL + L \leftrightarrow PL_2$  -governed by dissociation constants  $K_1$  and  $K_2$ , respectively- were simulated to yield the concentrations (relative to total fragment concentration  $P_T$ ) of species PL (circles),  $PL_2$  (squares) and their sum (triangles) in equilibrium for a value of  $K_1$  of 1  $\mu M$  and  $K_2$  values of 50 (blue), 100 (black) and 200  $\mu M$  (red). Total fragment  $P_T$  concentration was set to 100  $\mu M$ , and peptide  $L_T$  varies up to 350  $\mu M$ . In titration experiments, the peak height signal (inset to Figure 7) is assumed to follow a dependence on  $[PL] + [PL_2]$ , whereas the MWCS signal (Figure S4) would depend exclusively on  $[PL_2]$ .



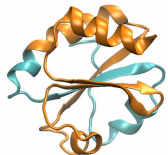
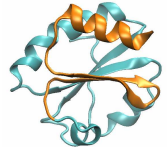
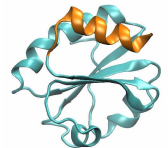
**Figure S6.** Regions of different transversal relaxation between the complex and full-length TRX.  $R_2$  values for residues 43-50 (helix  $\alpha_3$ ) and 74-89 (the  $\beta$  hairpin at the C-terminus of the fragment) are higher for the complex than for full-length TRX. The accessible surface area (calculated with a probe radius of 1.4 Å) for these residues in the fragment TRX1-93 (extracted from the PDB ID= 2TRX) is shown in yellow. A ribbon diagram of peptide TRX94-108 is shown in orange.





**Figure S7.** Far-UV CD spectra of isolated fragment TRX1-93. Fragment concentrations were 98, 73, 49, 25, and 10  $\mu\text{M}$ . Samples were prepared in 20 mM TrisHCl buffer, 100 mM NaCl, 1.0 mM DTT, pH 7.3 and spectra were acquired at 20 °C. In addition, the spectrum of the complex TRX1-93/TRX94-108 is shown as a reference. In this case, fragment concentration was 30  $\mu\text{M}$  and a 3:1 peptide to fragment molar ratio was used.

**Table S1. Complexes derived from *E. coli* thioredoxin (TRX).**

Complexes	Structural characterization method and redox state	Enzymic activity % of wild type TRX (substrate)	Dissociation constant $K_D$ $\mu\text{M}$ (temperature in $^{\circ}\text{C}$ ) method	References
<b>1-37/37-108</b> 	Secondary and tertiary structure:  47% and 35%, respectively; by CD.  Probably oxidized	0.1% (insulin)  15-20% (DTNB, TRXR)	6.5 (25), IT  4.0 (20), fluorescence quenching	2-4
<b>1-73/74-108</b> 	Full-structured; by CD,  fluorescence and NMR.  Probably oxidized	1% (insulin)  1% (DTNB, TRXR)	0.1 (20), sedimentation equilibrium  0.049 (20), fluorescence quenching	4, 5
<b>1-93/94-108</b> 	Full-structured; by CD  and fluorescence.  Reduced	7.1 % (Di-FTC-insulin)	12 (25), near-UV CD titration  2 (25), ITC  1.5 $\pm$ 1 (20) NMR titration  >150 (20), at or near the active site, NMR titration	7, 8 and this work

The N- and C- terminal fragments are depicted in cyan and orange, respectively. Abbreviations used are: CD, circular dichroism; Di-FTC-insulin, di-fluoresceinthiocarbamyl-insulin; DTNB, 5,5'-dithiobis(2-nitrobenzoic acid); ITC, isothermal titration calorimetry; TRXR, thioredoxin reductase.

**Table S2.** NMR peak assignments for TRX1-93.  $^{15}\text{N}$  and  $^1\text{H}$  amide chemical shifts for the reduced form of fragment  $^{13}\text{C}/^{15}\text{N}$  TRX1-93 (500  $\mu\text{M}$ ), in complex with peptide  $^{12}\text{C}/^{14}\text{N}$  TRX94-108 (1.5 mM) at 20  $^{\circ}\text{C}$ , 20 mM Tris-HCl, 100 mM NaCl, 1 mM DTT, pH 7.3.

Residue	$^{15}\text{N}\delta$ (ppm)	$\text{H}\delta$ (ppm)	Residue	$^{15}\text{N}\delta$ (ppm)	$\text{H}\delta$ (ppm)	Residue	$^{15}\text{N}\delta$ (ppm)	$\text{H}\delta$ (ppm)
Asp2	----	---	Gly33	----	---	Pro64	----	---
Lys3	118.7	8.39	Pro34	----	---	Gly65	112.6	10.27
Ile4	121.2	7.35	Cys35	115.2	8.00	Thr66	118.9	7.87
Ile5	125.7	8.26	Lys36	120.1	7.86	Ala67	124.1	9.78
His6	125.7	8.85	Met37	116.4	7.55	Pro68	----	---
Leu7	124.6	8.93	Ile38	122.7	8.29	Lys69	117.2	7.40
Thr8	108.1	8.18	Ala39	124.1	7.33	Tyr70	114.8	7.32
Asp9	119.7	8.21	Pro40	----	---	Gly71	107.9	7.51
Asp10	116.4	8.24	Ile41	117.4	6.78	Ile72	119.2	7.15
Ser11	118.0	8.30	Leu42	119.2	7.88	Arg73	128.1	8.65
Phe12	125.3	7.69	Asp43	118.7	7.35	Gly74	108.4	7.66
Asp13	117.3	8.74	Glu44	118.1	7.22	Ile75	114.4	8.17
Thr14	112.4	7.81	Ile45	120.7	8.53	Pro76	----	---
Asp15	118.8	8.46	Ala46	122.1	8.65	Thr77	118.8	7.88
Val16	112.8	7.59	Asp47	115.0	7.16	Leu78	125.8	8.92
Leu17	116.3	7.00	Glu48	120.7	8.66	Leu79	121.8	9.09
Lys18	115.1	7.41	Tyr49	115.3	8.77	Leu80	124.7	8.90
Ala19	122.4	6.61	Gln50	121.2	7.07	Phe81	128.1	9.99
Asp20	121.4	8.57	Gly51	115.7	9.28	Lys82	117.0	8.78
Gly21	108.7	8.18	Lys52	117.9	8.21	Asn83	124.1	9.44
Ala22	123.1	8.49	Leu53	119.5	7.86	Gly84	104.5	9.65
Ile23	120.9	9.17	Thr54	123.5	8.12	Glu85	118.6	7.84
Leu24	130.5	9.23	Val55	129.9	9.99	Val86	122.7	8.83
Val25	126.6	9.79	Ala56	129.6	9.34	Ala87	133.4	9.63
Asp26	125.8	8.87	Lys57	118.2	8.66	Ala88	117.5	7.77
Phe27	127.9	8.57	Leu58	123.6	9.00	Thr89	115.4	8.62
Trp28	120.0	8.31	Asn59	126.7	9.13	Lys90	126.9	9.10
Ala29	117.0	7.05	Ile60	122.5	8.60	Val91	126.6	8.65
Glu30	123.8	9.00	Asp61	122.1	7.68	Gly92	113.3	8.28
Trp31	111.0	6.64	Gln62	116.2	7.39	Ala93	127.3	7.53
Cys32	122.7	6.60	Asn63	115.3	7.41			

**Table S2.** Time course of complex TRX1-93/TRX94-108 formation followed by real-time NMR. The evolution of the intensity of  $^1\text{H}$ - $^{15}\text{N}$  backbone cross-peaks corresponding to 30 selected residues is shown here (for the full graphics, see Figure S2). Each kinetic curve could be accounted for by one exponential component. Non-linear fitting was performed with QtiPlot software, using the scaled Levenberg-Marquardt algorithm. Values for the kinetic constants together with their standard errors are shown below.

<b>Residue</b>	<b><math>k</math> (<math>\text{min}^{-1}</math>)</b>	<b>Residue</b>	<b><math>k</math> (<math>\text{min}^{-1}</math>)</b>
I4	$0.0099 \pm 0.0038$	D47	$0.0454 \pm 0.0141$
F12	$0.0073 \pm 0.0048$	G51	$0.0068 \pm 0.0044$
D13	$0.0198 \pm 0.0052$	A56	$0.0078 \pm 0.0031$
T14	$0.0188 \pm 0.0047$	A57	$0.0278 \pm 0.0093$
D15	$0.0214 \pm 0.0071$	N59	$0.0128 \pm 0.0050$
L17	$0.0125 \pm 0.0028$	G65	$0.0169 \pm 0.0040$
A19	$0.0191 \pm 0.0065$	K69	$0.0136 \pm 0.0030$
G21	$0.0275 \pm 0.0072$	Y70	$0.0086 \pm 0.0032$
I23	$0.0110 \pm 0.0050$	R73	$0.0133 \pm 0.0027$
V25	$0.0138 \pm 0.0048$	L78	$0.0109 \pm 0.0047$
A29	$0.0289 \pm 0.0109$	L79	$0.0190 \pm 0.0065$
E30	$0.0326 \pm 0.0092$	L80	$0.0182 \pm 0.0048$
C35	$0.0136 \pm 0.0040$	V86	$0.0149 \pm 0.0047$
I41	$0.0129 \pm 0.0040$	L88	$0.0122 \pm 0.0030$
I45	$0.0052 \pm 0.0020$	A93	$0.0089 \pm 0.0024$

## References

1. Chandrasekhar K, Campbell AP, Jeng MF, Holmgren A, and Dyson HJ. Effect of disulfide bridge formation on the NMR spectrum of a protein: studies on oxidized and reduced *Escherichia coli* thioredoxin. *J Biomol NMR* 1994; 4: 411-432.
2. Ghoshal AK, Swaminathan CP, Thomas CJ, Surolia A, and Varadarajan R. Thermodynamic and kinetic analysis of the *Escherichia coli* thioredoxin-C' fragment complementation system. *Biochem J* 1999; 339 ( Pt 3): 721-727.
3. Holmgren A. Thioredoxin-C': Reconstitution of an active form of *Escherichia coli* thioredoxin from two noncovalently linked cyanogen bromide peptide fragments. *FEBS Lett* 1972; 24: 351-354.
4. Yang XM, Georgescu RE, Li JH, Yu WF, Haierhan, and Tasayco ML. Recognition between disordered polypeptide chains from cleavage of an alpha/beta domain: self-versus non-self-association. *Pac Symp Biocomput* 1999; 590-600.
5. Tasayco ML, Fuchs J, Yang XM, Dyalram D, and Georgescu RE. Interaction between two discontinuous chain segments from the beta-sheet of *Escherichia coli* thioredoxin suggests an initiation site for folding. *Biochemistry* 2000; 39: 10613-10618.
6. Slaby I, and Holmgren A. Structure and enzymatic functions of thioredoxin refolded by complementation of two tryptic peptide fragments. *Biochemistry* 1979; 18: 5584-5591.
7. Santos J, Marino-Buslje C, Kleinman C, Ermacora MR, and Delfino JM. Consolidation of the thioredoxin fold by peptide recognition: interaction between *E. coli* thioredoxin fragments 1-93 and 94-108. *Biochemistry* 2007; 46: 5148-5159.
8. Santos J, Sica MP, Buslje CM, Garrote AM, Ermacora MR, and Delfino JM. Structural selection of a native fold by peptide recognition. Insights into the thioredoxin folding mechanism. *Biochemistry* 2009; 48: 595-607.

